Time Dependence of 50–250 MeV Galactic Cosmic-Ray Protons between Solar Cycles 24 and 25, Measured by the High-energy Particle Detector on board the CSES-01 Satellite

M. Martucci[1], R. Ammendola[1], D. Badoni[1], S. Bartocci[1], R. Battiston[2,3], S. Beolè[4,5], W. J. Burger[2],
D. Campana[6], G. Castellini[7], P. Cipollone[1], S. Colì[4], L. Conti[1,8], A. Contin[9,10], M. Cristoforetti[2,11],
G. D'Angelo[12], C. De Donato[1], C. De Santis[1], A. Di Luca[2,11], F. M. Follega[2,3], G. Gebbia[2,3], R. Iuppa[2,3], A. Lega[2,3],
M. Lolli[10], N. Marcelli[13], G. Masciantonio[1], M. Mergè[1,14], M. Mese[6,15], C. Neubüser[2], F. Nozzoli[2], A. Oliva[9,10],
G. Osteria[6], L. Pacini[16], F. Palma[1], F. Palmonari[9,10], B. Panico[6,15], A. Parmentier[1,12], S. Perciballi[4,5], F. Perfetto[17],
P. Picozza[1,18], M. Pozzato[10], G. M. Rebustini[1,18], E. Ricci[2,3], M. Ricci[19], S. B. Ricciarini[7], U. Savino[4,5],
Z. Sahnoun[10], V. Scotti[6,15], A. Sotgiu[1], R. Sparvoli[1,18], P. Ubertini[12], V. Vilona[2], V. Vitale[1], S. Zoffoli[14],
P. Zuccon[2,3], O. P. M. Aslam[20], M. D. Ngobeni[21], and M. S. Potgieter[20,22]

[1] INFN-Sezione di Roma "Tor Vergata," Via della Ricerca Scientifica 1, I-00133 Roma, Italy; matteo.martucci@roma2.infn.it
[2] INFN-TIFPA, V. Sommarive, I-38123 Povo (Trento), Italy
[3] University of Trento, V. Sommarive 14, I-38123 Povo (Trento), Italy
[4] INFN-Sezione di Torino, Via P. Giuria 1, I-10125 Torino, Italy
[5] University of Torino, Via P. Giuria 1, I-10125 Torino, Italy
[6] INFN-Sezione di Napoli, V. Cintia, I-80126, Napoli, Italy
[7] IFAC-CNR, V. Madonna del Piano, 10, I-50019 Sesto Fiorentino (Firenze), Italy
[8] Uninettuno University, C.so V. Emanuele II, 39, I-00186, Roma, Italy
[9] University of Bologna, V.le Berti Pichat 6/2, Bologna, Italy
[10] INFN-Sezione di Bologna, V.le Berti Pichat 6/2, Bologna, Italy
[11] Fondazione Bruno Kessler, V. Sommarive 18, I-38123 Povo (Trento), Italy
[12] INAF-IAPS, V. Fosso del Cavaliere 100, I-00133, Roma, Italy
[13] INFN-Sezione di Trieste, Galleria Padriciano, 99, I-34149 Trieste, Italy
[14] Italian Space Agency, V. del Politecnico, I-00133 Roma, Italy
[15] University of Napoli "Federico II," V. Cintia, I-80126, Napoli, Italy
[16] INFN-Sezione di Firenze, V. Sansone 1, I-50019 Sesto Fiorentino (Firenze), Italy
[17] INFN-Sezione di Napoli, I-80126, Napoli, Italy
[18] University of Roma "Tor Vergata," Via della Ricerca Scientifica 1, I-00133 Roma, Italy
[19] INFN-LNF, V. E. Fermi, 54, I-00044 Frascati (Roma), Italy
[20] Shandong Institute of Advanced Technology (SDIAT), 250100 Jinan, Shandong Province, People's Republic of China
[21] Centre for Space Research, North-West University, 2520 Potchefstroom, South Africa
[22] Institute for Experimental and Applied Physics, Christian-Albrechts University in Kiel, D-24118 Kiel, Germany

Abstract

Time-dependent energy spectra of galactic cosmic rays (GCRs) carry crucial information regarding their origin and propagation throughout the interstellar environment. When observed at the Earth, after traversing the interplanetary medium, such spectra are heavily affected by the solar wind and the embedded solar magnetic field permeating the inner sectors of the heliosphere. The activity of the Sun changes significantly over an 11 yr solar cycle—and so does the effect on cosmic particles; this translates into a phenomenon called solar modulation. Moreover, GCR spectra during different epochs of solar activity provide invaluable information for a complete understanding of the plethora of mechanisms taking place in various layers of the Sun's atmosphere and how they evolve over time. The High-Energy Particle Detector (HEPD-01) has been continuously collecting data since 2018 August, during the quiet phase between solar cycles 24 and 25; the activity of the Sun is slowly but steadily rising and is expected to peak around 2025/2026. In this paper, we present the first spectra for ∼50–250 MeV galactic protons measured by the HEPD-01 instrument—placed on board the CSES-01 satellite—from 2018 August to 2022 March over a one-Carrington-rotation time basis. Such data are compared to the ones from other spaceborne experiments, present (e.g., EPHIN, Parker Solar Probe) and past (PAMELA), and to a state-of-the-art three-dimensional model describing the GCRs propagation through the heliosphere.

Unified Astronomy Thesaurus concepts: Active sun (18); Heliosphere (711); Galactic cosmic rays (567)

1. Introduction

Galactic cosmic rays (GCRs) are originated outside the solar system and then accelerated by energetic processes in the interstellar medium, showing a time-independent and isotropic distribution when arriving at the heliopause (Fisk & Gloeckler 2012; Blasi 2013, 2014; Amato & Blasi 2018). However, after entering the heliosphere, the energy distributions of GCRs are modified by the turbulence in the solar wind. This plasma of ionized gas (Parker 1958) is continuously expanding from the corona of the Sun at supersonic speed into space, and it carries an embedded magnetic field into the solar system, generating the heliospheric magnetic field (HMF). Moreover, given that the activity of the Sun follows an 11 and 22 yr periodicity (Usoskin 2017)—of which the number of visible

sunspots appearing over the solar disk is one of the most used proxies (Ross & Chaplin 2019)—changes in galactic particle fluxes show a very clear time dependence (e.g., Heber 2013; Potgieter 2013) in response to the significant variation of the configuration of the HMF. During a period of minimum activity, the solar magnetic field structure is regular and spatially ordered, while, during maximum phases, it assumes a more chaotic configuration—also undergoing a polarity reversal. This phenomenon is referred to as solar modulation (Parker 1965; Gleeson & Axford 1968). Since the end of the last century, there has been a plethora of new and advanced measurements of energy spectra and composition of the GCR population, with a consequently notable improvement in the precision and reduction of overall uncertainties (Boezio et al. 2020). This is particularly true for the most abundant species inside the cosmic radiation, i.e., proton and helium nuclei (Panov et al. 2009; Adriani et al. 2011; Aguilar et al. 2015; Yoon et al. 2017; Adriani et al. 2019; An et al. 2019). However, from a more fundamental point of view, even if it is important to gain knowledge of the GCR spectrum beyond the heliopause—known as the local interstellar spectrum or LIS (Stone et al. 2013, 2019)—to look for evidence of new physics (Donato et al. 2009; Blum et al. 2013), it is the modulated spectrum that has the greatest impact at Earth Song et al. 2021. For this reason, the information provided by experimental data, past and present (Potgieter 2013; Potgieter et al. 2014), is essential to guarantee a more precise understanding of the transport of galactic particles throughout the heliosphere. From these data, it is possible to gather a unique insight on the properties and patterns of the HMF and the heliosphere as a whole. On the other hand, an increasing number of numerical models, most of which based on solving the transport equation for the heliosphere, have been recently developed (Vos & Potgieter 2015, 2016; Boschini et al. 2019; Corti et al. 2019; Shen et al. 2019) to study various physical processes involved in solar modulation, i.e., diffusion, particle drift, convection, and adiabatic energy changes (Quenby 1984; Kóta 2013; Potgieter 2013, 2017). To validate these models, experiments are needed to perform precise and prolonged observations of GCR populations over one or more solar cycles. From another point of view, the interactions between high-energy ionized particles like protons and the instruments on board spacecraft are known to be a concern in planning future interplanetary missions, since these particles may cause in-orbit failures and they may penetrate spacecraft shielding to interact with the biological tissue of human crews, steeply increasing health risks for astronauts. Therefore, having clear measurements of particle fluxes in the cosmic environment is pivotal for the future of the space age. In this framework, the High-Energy Particle Detector (HEPD-01), launched in 2018, sets out to do all of that, exploiting its potential for cosmic-ray measurements at energies below a few hundred MeV. HEPD-01—together with its successor (HEPD-02) planned to be launched in 2023—is capable of monitoring the evolution of the current solar cycle in an energy range that is not covered by current missions; furthermore, HEPD-01 is bridging the measurements done by low-energy (SOHO/EPHIN, Parker Solar Probe (PSP)/High Energy Telescope, PSP/Low Energy Telescope) and high-energy (Alpha Magnetic Spectrometer (AMS-02), CALET, DAMPE) experiments, also covering part of the energy range of the past mission PAMELA, providing an important comparison with measurements of previous solar cycles (Adriani et al. 2013; Martucci et al. 2018; Marcelli et al. 2020, 2022).

2. Limadou Mission and the HEPD-01 Detector

The CSES satellite (Shen et al. 2018) was launched on 2018 February 2, and is currently flying on a Sun-synchronous polar orbit at a ∼507 km altitude, a 97° inclination, and a 5 day revisiting periodicity. It is the first of a network of multi-instrument satellites scheduled for launch in a few years. The mission objectives include monitoring of the electromagnetic field, plasma, and particle perturbations in the ionosphere and magnetosphere, either due to natural sources, like earthquakes or solar events, or artificial emitters. The orbital characteristics of CSES allow for a detailed investigation of the high-latitude regions of the Earth—the ones more sensitive to the influence of the Sun, despite the fact that all payloads are switched off above +65° and below −65° of latitude; these limitations were relaxed at the end of 2019 to +70° and −70°, respectively. The High-Energy Particle Detector is one of the nine instruments on board the satellite; it was completely designed and integrated in Italy in the framework of the CSES/Limadou project. It is a light and compact payload (40.36 × 53.00 × 38.15 cm, total mass ∼45 kg), made up of a series of subdetectors: from the top of the detector, two double-sided silicon microstrips planes (213.2 × 214.8 × 0.3 mm) providing tracking information, a single layer of EJ-200 segmented plastic scintillator (six paddles, 20 × 3 × 0.5 cm each), a range calorimeter for energy measurement, composed of a stack (TOWER) of 16 plastic scintillators, $P_1...P_{16}$ (15 × 15 × 1 cm), and, finally, a 3 × 3 matrix of lutetium-yttrium oxyorthosilicate (LYSO) inorganic scintillator crystals (5 × 5 × 4 cm). The instrument is surrounded—laterally and at the bottom—by five plastic scintillators that reject out-of-acceptance particles or particles that do not deposit all their energy inside the detector (VETO). The payload is optimized to measure electrons in the 3–100 MeV energy range, and protons between ∼40 and 250 MeV, as well as light nuclei with a ±60° field of view and a geometrical acceptance of more than 400 cm² sr. The HEPD-01 capabilities for galactic and trapped protons and space weather studies have already been assessed in Bartocci et al. (2020), Martucci et al. (2022), Palma et al. 2021, and in Piersanti et al. (2022). More technical details on the mission and the instrument itself can be found in previous publications (Picozza et al. 2019; Ambrosi et al. 2020; Sotgiu et al. 2020; Ambrosi et al. 2021).

3. Data Analysis

Data analysis and methodology for GCR proton estimation in this paper is mostly unchanged from the original one that has been employed in Bartocci et al. (2020) to obtain differential spectra in 6 month intervals. For this reason, in this section, only a summary will be given to the reader. The differential energy spectrum $\Phi(E)$ was evaluated as follows:

$$\Phi(E) = \frac{N(E)}{\epsilon(E) \times G(E) \times LT \times \Delta E}, \quad (1)$$

where $N(E)$ is the number of good proton candidates in the sample, $\epsilon(E)$ the efficiency of the various proton selections, $G(E)$ the geometrical factor or acceptance, LT the instrumental live time, and ΔE the width of the energy interval. In order to
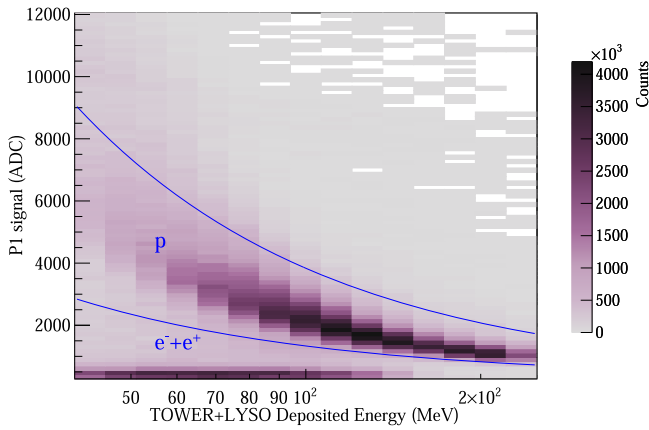
Figure 1. Proton and electrons+positrons signal on plane P_1 as a function of the total energy deposited inside the calorimeter (TOWER+LYSO). To better visualize the separation in the plot, only vertical particles have been selected. The blue curves identify the selection employed to discriminate between protons and other populations.

give a valid trigger to start data acquisition, a proton must cross one of the paddles of the trigger plane (then we require offline a single paddle hit to avoid multiparticle events and reduce secondaries) and at least the first two planes of the TOWER, P_1 and P_2. After a valid trigger is acquired, only particles contained (namely, fully stopping inside the TOWER+LYSO subdetector) are included in the flux sample, discarding the ones generating a signal in one of the VETO planes. To discriminate between protons and electron/positron populations, a double-curve selection—each one with the form $y_i \propto \frac{A_i}{x}$ with A_i a constant—is required on the signal deposited on the first TOWER plane (P_1) as a function of the total deposited energy. The P_1 signal distribution as a function of the total energy lost in the TOWER+LYSO subdetector is shown in Figure 1, while the blue curves represent the 15% and 95% quantile threshold used to select the proton band. Other auxiliary selections are applied to further clean the sample (Bartocci et al. 2020).

After the latitude at which HEPD-01 was switched off was increased to ±70°, more particles were collected in low-cutoff sectors of the orbit, consequently increasing the statistics of the sample. For what concerns the geomagnetic selection, in this work we estimated the McIlwain parameter L—hereafter L shell—using the Altitude-Adjusted Corrected Geomagnetic coordinates reference frame (Stephens et al. 2017). Only portions of the CSES orbit that were above a value of the L shell greater than 7 were selected, to assure that all coming protons with energy >50 MeV were of cosmic origin (i.e., above the cutoff threshold); the same selection was consequently applied to the estimation of the live time, for consistency. We used a single map for the entire period 2018–2022, after checking the stability (on average) of the geomagnetic environment over a year-by-year basis. Indeed, it turned out that, only during major solar events—like the one observed by HEPD-01 in Martucci et al. (2023), the disturbance of the magnetic field of the Earth was high enough to affect ∼50–60 MeV proton populations. However, these periods were excluded from the analysis, as mentioned before. We also cross-checked our results with the static rigidity cutoff map—obtained with the Tsyganenko 96 magnetospheric

model (Tsyganenko 1995), already used in Bartocci et al. (2020).

The geometrical factor of HEPD-01 was evaluated using a Monte Carlo simulation of isotropically generated ($0° < \theta < 90°$ and $0° < \phi < 180°$) protons with primary energy ranging from 1 MeV to 10 GeV; such simulation was performed using a GEANT4-based software (Agostinelli et al. 2003), together with a carefully crafted digitization procedure, tuned with test beam and flight data. The resulting total instrumental efficiency and the overall contamination by inclined, >40 MeV minimum ionizing particle–like electrons were both evaluated using the digitized Monte Carlo simulation. The proton energy spectrum measured in the entire calorimeter was corrected to account for particle slowdown and energy loss in passive structures covering the sensitive materials of the apparatus; this was accomplished by employing a Bayesian approach unfolding (D'Agostini 1995, 2010). As already described in detail in Bartocci et al. (2020), possible sources of systematic uncertainties lie in both the deconvolution procedure and on the differences between flight data and Monte Carlo. The single proton fluxes were evaluated on a Carrington rotation (CR) basis, which means ∼27 days. The present analysis spans the period between Carrington rotation 2207 and 2255 (from 2018 August up to 2022 March). However, some of these experimental observations took place during a period of high solar activity characterized by numerous flares and solar energetic particle (SEP) events. A significant fraction of these events produced high-energy protons (one even reaching the ∼GeV threshold), which reached the Earth orbit and were indistinguishable from the GCR component collected by HEPD-01. For a proper study of the solar modulation of GCRs, this solar component had to be excluded; the approach used in this work was to directly remove the periods in which this contamination was present. Also, the periods of Forbush decreases (Forbush 1937) were excluded from the analysis. For this last kind of phenomena, we employed data from various Neutron Monitor at different locations, extracted from the NMDB Event Search Tool at https://www.nmdb.eu/nest/search.php to isolate periods in which a sudden variation of the GCR flux with respect to a quiet background was evident. Furthermore, as a cross-check, the duration of these time intervals—usually a few days—was compared with the one observed in our data at low energies (where the disturbance due to the Forbush effect normally lasts longer); finally, these periods of time were removed.

4. Results

A total of 49 proton energy spectra were obtained from 2018 August up to 2022 March, during an initial phase of minimum activity, before 2020 July, and a subsequent rise toward the maximum phase—from the second half of 2020 onward. However, CR number 2218 is excluded due to an internal system shutdown, while CR numbers 2238, 2244, 2245, 2246, 2248, 2249, 2250, 2253, 2254, and 2255 are missing because of the presence of heavy and prolonged solar proton contamination, as previously explained in Section 3. HEPD-01 data points of differential proton spectra in four CRs (2207, 2225, 2239, and 2252) are listed in Table 1. A global picture of energy and time dependence of GCR protons is depicted in Figure 2 for the period 2018–2022, between 0.050 and 0.250 GeV. The colored bar on the right refers to the respective CR number, from 2207 (blue) to 2255 (red).

Table 1
HEPD-01 Differential Proton Spectra in Four Different CRs, together with Both Statistical and Systematic Uncertainties

Energy Bin (GeV)	$(m^2\ s\ sr\ GeV)^{-1}$ CR 2207	Flux ±Stat Err. ±Syst Err.		
		$(m^2\ s\ sr\ GeV)^{-1}$ CR 2225	$(m^2\ s\ sr\ GeV)^{-1}$ CR 2239	$(m^2\ s\ sr\ GeV)^{-1}$ CR 2252
0.050–0.059	886.03 ± 62.96 ± 125.42	1002.97 ± 80.60 ± 141.97	1180.28 ± 89.92 ± 167.07	961.01 ± 87.65 ± 136.03
0.059–0.069	985.57 ± 81.03 ± 133.83	1175.29 ± 98.66 ± 159.59	1308.80 ± 110.05 ± 177.73	1122.02 ± 104.84 ± 152.36
0.069–0.081	1120.22 ± 77.79 ± 92.01	1319.57 ± 85.86 ± 108.39	1488.44 ± 91.31 ± 122.26	1331.76 ± 83.65 ± 109.39
0.081–0.095	1333.04 ± 70.07 ± 205.52	1600.91 ± 76.47 ± 246.82	1695.38 ± 79.04 ± 261.39	1498.22 ± 73.06 ± 230.99
0.095–0.112	1429.33 ± 85.12 ± 143.83	1838.17 ± 90.41 ± 184.97	1936.48 ± 92.40 ± 194.86	1696.24 ± 84.76 ± 170.69
0.112–0.131	1688.78 ± 107.33 ± 112.84	1933.65 ± 115.93 ± 129.20	2123.24 ± 117.09 ± 141.87	1880.89 ± 108.47 ± 125.68
0.131–0.154	1875.75 ± 130.58 ± 135.17	2141.64 ± 152.82 ± 154.33	2361.53 ± 153.21 ± 170.17	1992.23 ± 146.25 ± 143.56
0.154–0.181	1991.76 ± 155.98 ± 95.72	2358.9 ± 194.39 ± 113.36	2621.29 ± 202.29 ± 125.97	2234.29 ± 194.60 ± 107.37
0.181–0.213	2224.79 ± 155.13 ± 209.32	2633.99 ± 177.54 ± 247.82	2891.20 ± 181.77 ± 272.02	2437.40 ± 173.05 ± 229.32
0.213–0.250	2321.07 ± 259.40 ± 328.60	2897.53 ± 287.05 ± 410.21	3101.31 ± 283.98 ± 439.06	2770.21 ± 270.09 ± 392.19
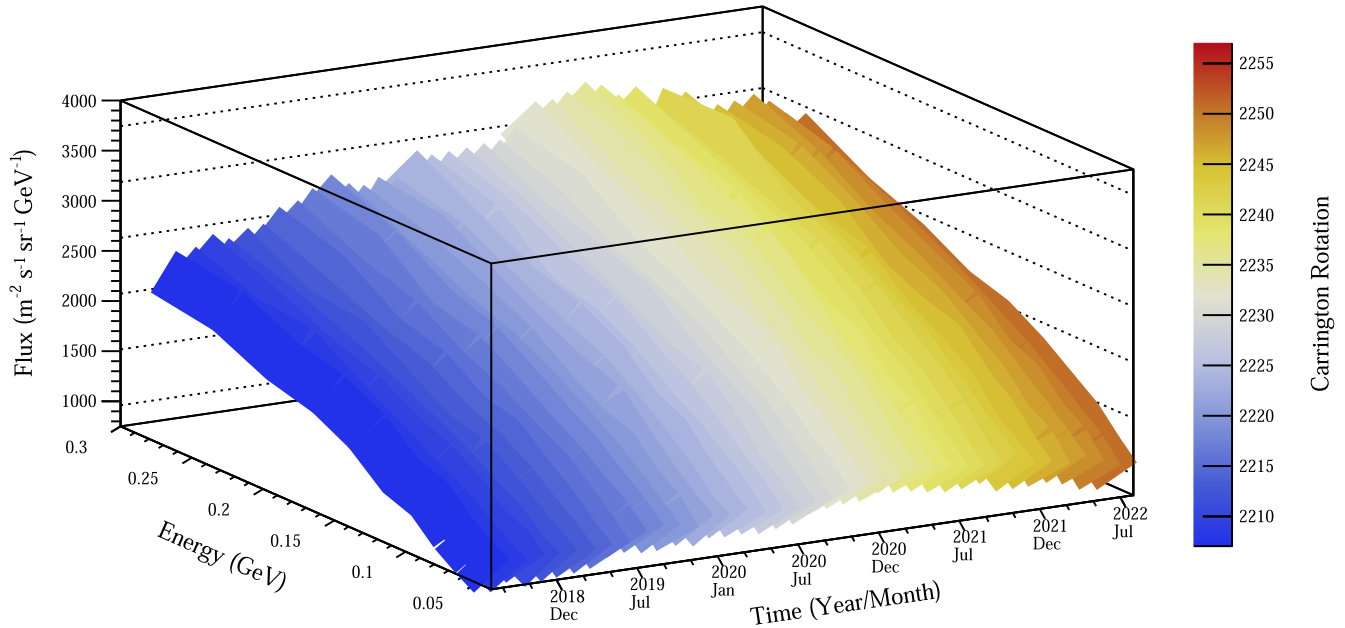
Figure 2. Evolution of HEPD-01 GCR protons as a function of energy and time between 2018 and 2022 (CRs 2207-2255). It is clear how spectra slowly rise before 2020 July, to start decreasing from the second half of 2020 onward.

The time dependence is evident and this is particularly well visible in Figure 3 (upper panel). Here, the time profiles of GCR protons measured by HEPD-01 in 10 energy intervals from ∼0.050 to ∼0.250 GeV between 2018 August and 2022 March are reported. During the period between May and 2020 July, proton flux reaches its maximum value ($>3300\ m^{-2}\ s^{-1}\ sr^{-1}\ GeV^{-1}$ for ∼0.250 GeV protons and ∼1200 $m^{-2}\ s^{-1}\ sr^{-1}\ GeV^{-1}$ for ∼0.050 GeV). Errors in each data point account for both statistical and systematic uncertainties. In the bottom panel, the sunspot number (red) and Heliographic Current Sheet or HCS (blue) tilt angle (Hoeksema 1992) are shown. The former is taken from https://www.sidc.be/silso/datafiles, while the latter—obtained with radial boundary conditions—is taken from the Wilcox Solar Observatory at http://wso.stanford.edu. The HCS tilt angle represents the misalignment of the magnetic dipole axis of the Sun with respect to the solar rotational axis and is one of the best proxies for modulation of charged particles in cosmic rays because its time variations are related globally to the solar magnetic field. From late 2018, the tilt angle gradually decreased until mid-2020, when it started increasing from low values (typical for a period of solar

minimum activity) showing a rapid and steep rise around late 2021. During this entire period, the flux of ∼0.050 GeV protons gradually increased by ∼30% and it subsequently decreased by about 20%, while the flux of ∼0.250 GeV protons increased by ∼40% and it decreased by ∼10%. Usually, lower energies are more affected by modulation with respect to the higher ones, but—due to the limited energy span of the HEPD-01 detector and the high systematic uncertainties—our data do not show such clear energy dependence.

As a useful reference, in Figure 4, HEPD-01 data on CR 2233 (July 15—2020 August 11) are reported together with three proton spectra from the PAMELA detector (Picozza et al. 2007), two obtained during solar minimum conditions of cycle 23—2006 and 2009—and one from 2014, during the maximum phase of cycle 24 (Adriani et al. 2013; Martucci et al. 2018). As can be seen, the spectrum from HEPD-01 in 2020 is higher than the one from PAMELA in 2009 despite similar minimum solar activity.

Concerning this current solar cycle, other spaceborne experiments are taking data in the few-tens MeV sector of the GCR spectrum; however, HEPD-01 offers a higher
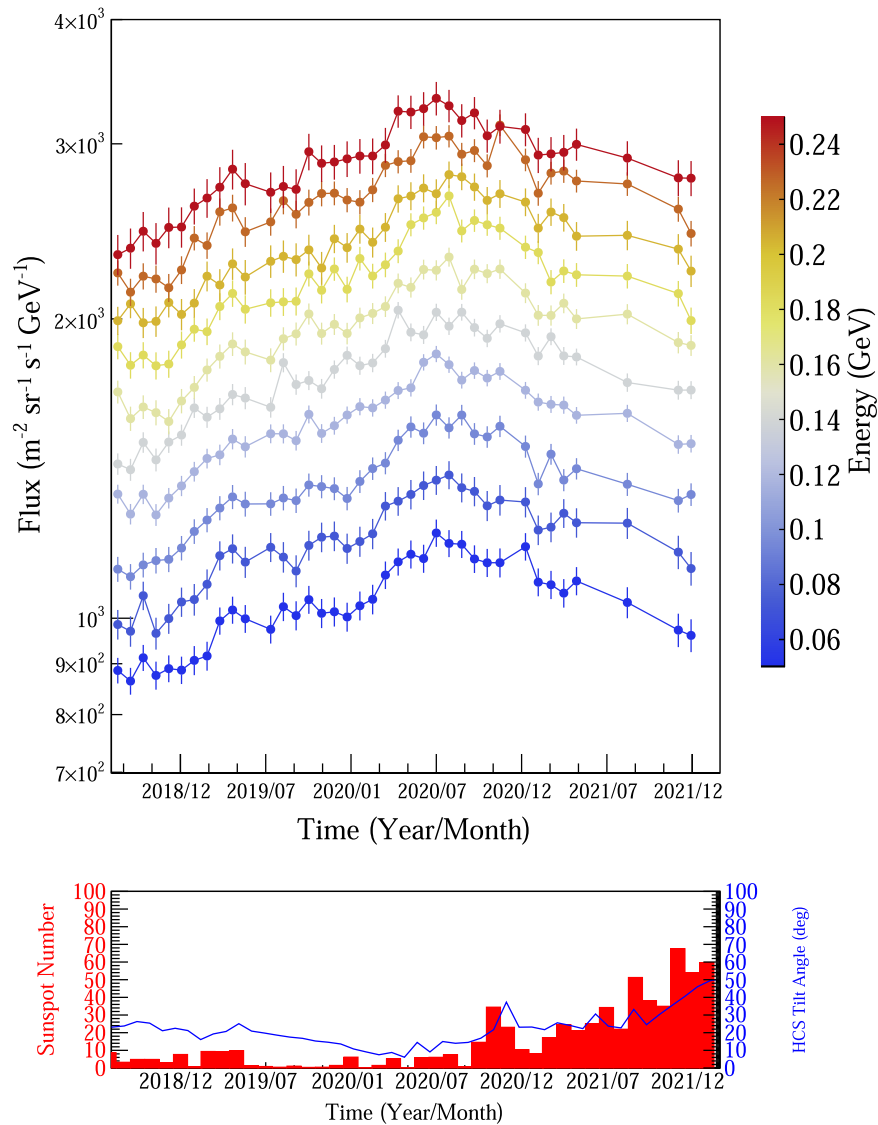
Figure 3. Time profile of GCR protons measured by HEPD-01 in 10 energy intervals (upper panel) between 2018 and 2022. Error bars take into account both statistical and systematic uncertainties. Sunspot number (red) and HCS tilt angle values (blue) as a function of time, in the same period (bottom panel).

precision and more stability over time with respect to the others. This can be seen in Figure 5, where GCR protons measured by HEPD-01 between 2018 October 26 and 2018 November 23 (left panel), and between 2021 November 18 and 2021 December 15 (right panel) are depicted together with data from the EPHIN detector on board SOHO (Müller-Mellin et al. 1995) and the IS⊙IS suite on board the Parker Solar Probe (Fox et al. 2016; McComas et al. 2016). The >0.050 GeV threshold of HEPD-01 allows for fewer possibilities of contamination by solar protons from SEPs, allowing a more continuous monitoring of the GCR proton population over time without external disturbances.

5. Discussion and Conclusions

The HEPD-01 detector, in the framework of the CSES/ Limadou mission, has been observing GCR protons since mid-2018, monitoring the time dependence of their spectra below a few hundred MeV. In this work, we present a collection of such proton spectra from 2018 August to 2022 March, with a time resolution of a single Carrington rotation, integrating and

expanding previously published results (Bartocci et al. 2020). During this period—from CR 2207 to CR 2255—the solar cycle 24 came to an end, cycle 25 began to rise and HEPD-01 observations allowed to follow changes in modulation effects near a minimum condition (when spectra became higher) and also during the first months leading to a maximum (where fluxes started gradually decreasing). Figure 2 summarizes the variation of these spectra over the entire period, both as a function of time and energy; the peak of the fluxes is reached around May/2020 July, meaning that the Sun was in its most quiet condition. This can also be seen in Figure 4, where the GCR proton spectrum in mid-2020 appears to be higher than the one measured by PAMELA in 2009 December, which is considered the most quiet period of solar cycle 23. It has been shown that during the minimum phases of many solar cycles, when the sunspot number is the lowest, several factors can affect GCR modulation inside the heliosphere; solar wind velocity, HMF magnitude in both toroidal/poloidal branches, and HCS tilt angle are among them. Figure 4 is direct proof that, even during this solar cycle, these factors and the relations between them could lead to maxima in GCR flux intensities.
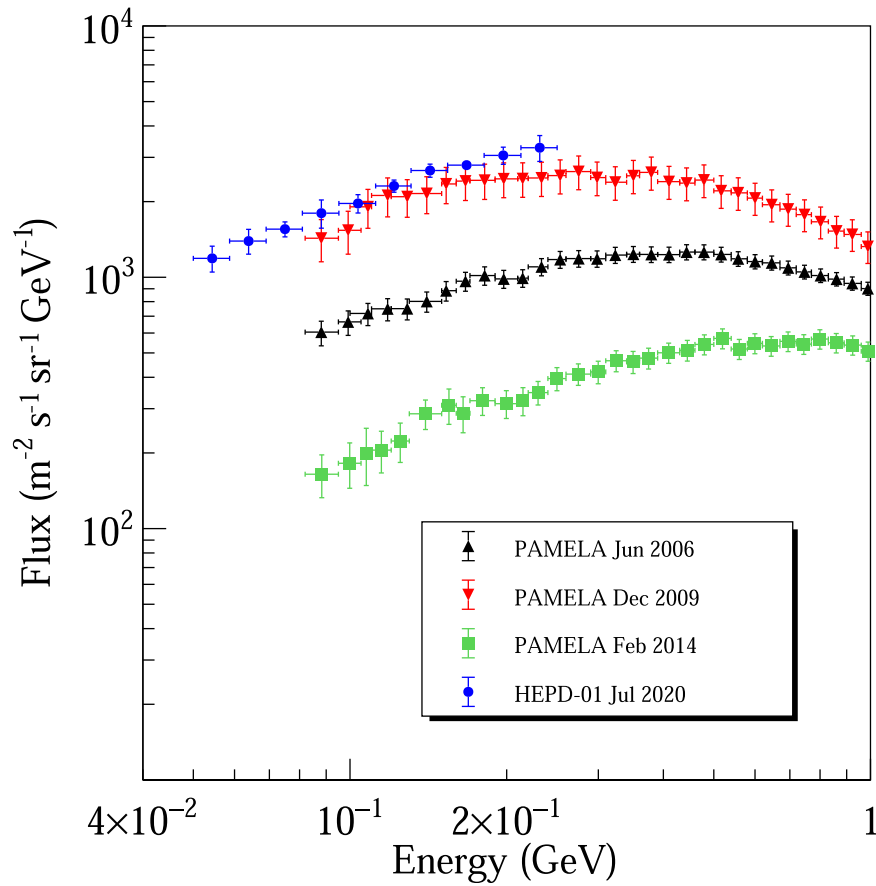
Figure 4. HEPD-01 data on CR 2233 (2020 July) together with three proton spectra from the PAMELA detector—2006 June (black), 2009 December (red), and February 2014 (green). As can be seen, the spectrum from HEPD-01 is higher than the one from 2009 by PAMELA.
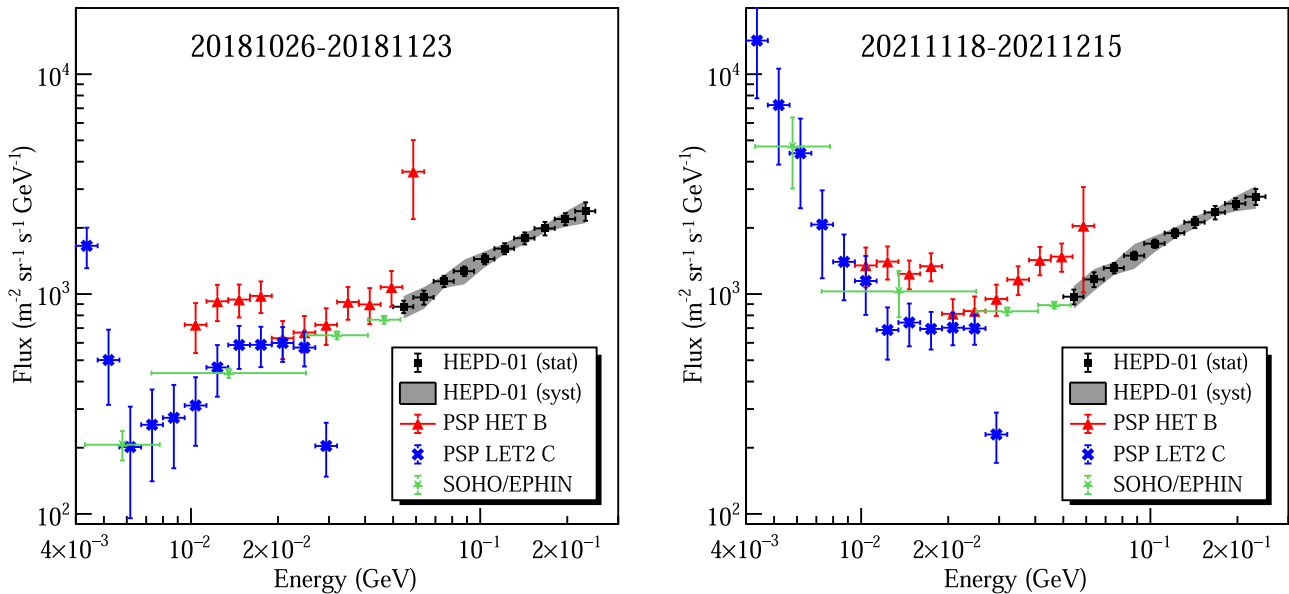
Figure 5. GCR proton spectra by HEPD-01 between 2018 October 26 and 2018 November 23 (left panel) and between 2021 November 18 and 2021 December 15 (right panel), together with proton data—in the same time intervals—from the EPHIN detector on board SOHO and the IS☉IS suite on board the Parker Solar Probe.

This statement is true not only for cycles 23, 24, and 25, but also for the previous five cycles (Potgieter & Vos 2017; Krainev et al. 2021). The time dependence of GCR protons at energies ~50–250 MeV with good resolution and preciseness presented in Figure 3 is also ideal for investigating features of solar modulation occurring at lower energies with appropriate

theoretical and numerical models. These HEPD-01 fluxes can be utilized to adjust modulation models for moderate to low solar activity conditions in the heliosphere. This can be achieved with our current comprehensive model (Potgieter & Vos 2017) which is based on solving numerically the transport equation (TPE)—derived by Parker in Parker (1965)—in 3D,
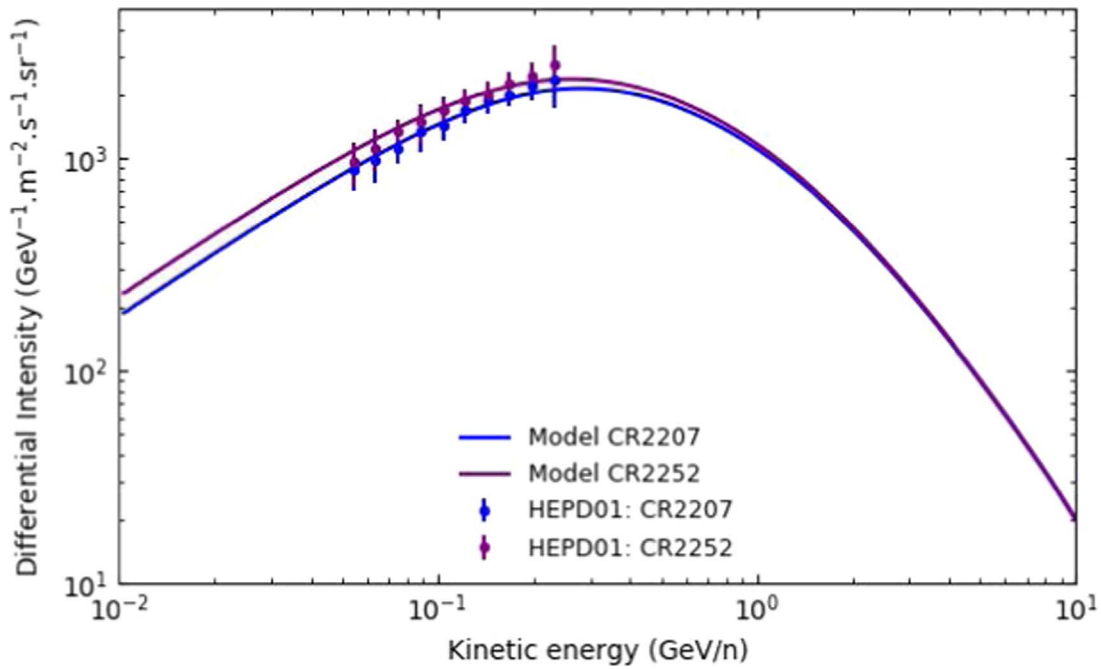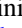
Figure 6. Computed proton fluxes as a function of kinetic energy for CR 2207 (purple solid line) and CR 2252 (blue solid line) at the Earth are shown together with the corresponding measured fluxes from HEPD-01 (circles).

with coordinates r, θ, and ϕ as a function of rigidity (kinetic energy) and solar modulation proxies. The TPE contains four major modulation processes: convection, diffusion, adiabatic energy changes, and gradient, curvature, and current sheet drifts. Combined, these interplaying processes cause the shape of GCR proton spectra, and so is other GCR species, to change over the two magnetic polarity cycles, mainly because of particle drifts. It is important to note that to successfully model GCR spectra, assumptions about the LIS, shape of the heliosphere, HMF and its polarity, solar wind velocity, HCS tilt angle, and elements of the diffusion and drift tensor must be specified beforehand in the model. In our 3D model, the expressions for the diffusion and drift coefficients used for the computations, as well as other relevant heliospheric parameters and proxies, are described in detail in Ngobeni et al. (2020), Aslam et al. (2021), and Potgieter et al. (2021). Figure 6 depicts the computed proton spectra overlaid on the corresponding observed HEPD-01 spectra for CR 2207 and CR 2252. The essence of this figure is to show that the HEPD-01 proton spectra are well reproduced—inside the instrumental systematic uncertainties—by our numerical model for the entire extension of the spectrum, settling into the expected adiabatic regime at these energies. Moreover, a comparison with GCR proton data from AMS-02 (Aguilar et al. 2021), with energies above ~1 GeV, will be the subject of a forthcoming paper. The true maximum of solar activity of cycle 25 is expected to peak around late 2025–early 2026, when hopefully two detectors like HEPD-01 and HEPD-02 will be taking high-precision data—especially if compared with data from other experiments (see Figure 5)—of GCR populations at low-Earth orbit, allowing for a continuous monitoring of the conditions of the heliosphere over almost an entire solar cycle. HEPD-02 will be put in the same orbit plane—with a 180° phase difference—and it will also have a concurrent trigger system (allowing for lower energy measurements). Moreover, it will increase angular and energy resolutions and it will be fully operational even above the polar caps, highly increasing the available statistics.

ORCID iDs

M. Martucci ◉ https://orcid.org/0000-0002-3033-4824
R. Ammendola ◉ https://orcid.org/0000-0003-4501-3289
D. Badoni ◉ https://orcid.org/0000-0002-9027-2039
S. Bartocci ◉ https://orcid.org/0000-0002-3066-8621
R. Battiston ◉ https://orcid.org/0000-0002-5808-7239
S. Beolè ◉ https://orcid.org/0000-0003-4673-8038
W. J. Burger ◉ https://orcid.org/0000-0003-1977-6354

D. Campana https://orcid.org/0000-0003-1504-9707
G. Castellini https://orcid.org/0000-0002-0177-0643
P. Cipollone https://orcid.org/0000-0003-3903-290X
S. Coli https://orcid.org/0000-0001-7470-4463
L. Conti https://orcid.org/0000-0003-2966-2000
A. Contin https://orcid.org/0000-0002-2535-5700
M. Cristoforetti https://orcid.org/0000-0002-0127-1342
C. De Donato https://orcid.org/0000-0002-9725-1281
C. De Santis https://orcid.org/0000-0002-7280-2446
F. M. Follega https://orcid.org/0000-0003-2317-9560
G. Gebbia https://orcid.org/0000-0001-7252-7416
R. Iuppa https://orcid.org/0000-0001-5038-2762
N. Marcelli https://orcid.org/0000-0001-9375-735X
G. Masciantonio https://orcid.org/0000-0002-8911-1561
M. Mergè https://orcid.org/0000-0002-2018-4236
C. Neubüser https://orcid.org/0000-0002-2008-8404
F. Nozzoli https://orcid.org/0000-0002-4355-7947
A. Oliva https://orcid.org/0000-0002-6612-6170
G. Osteria https://orcid.org/0000-0002-9871-8103
L. Pacini https://orcid.org/0000-0001-6808-9396
F. Palma https://orcid.org/0000-0001-7076-8830
F. Palmonari https://orcid.org/0000-0003-3707-0013
B. Panico https://orcid.org/0000-0003-1063-6961
A. Parmentier https://orcid.org/0000-0002-9073-3288
F. Perfetto https://orcid.org/0000-0001-8119-5046
P. Picozza https://orcid.org/0000-0002-7986-3321
M. Pozzato https://orcid.org/0000-0003-0279-5436
G. M. Rebustini https://orcid.org/0000-0001-8587-592X
E. Ricci https://orcid.org/0000-0002-4222-9976
M. Ricci https://orcid.org/0000-0001-6816-4894
S. B. Ricciarini https://orcid.org/0000-0001-6176-3368
U. Savino https://orcid.org/0000-0003-1884-2444
Z. Sahnoun https://orcid.org/0000-0003-1176-2003
V. Scotti https://orcid.org/0000-0001-8868-3990
A. Sotgiu https://orcid.org/0000-0001-8835-2796
R. Sparvoli https://orcid.org/0000-0002-6314-6117
P. Ubertini https://orcid.org/0000-0003-0601-0261
V. Vilona https://orcid.org/0000-0001-9893-9419
V. Vitale https://orcid.org/0000-0001-8040-7852
P. Zuccon https://orcid.org/0000-0001-6132-754X
O. P. M. Aslam https://orcid.org/0000-0001-9521-3874
M. D. Ngobeni https://orcid.org/0000-0001-5844-3419
M. S. Potgieter https://orcid.org/0000-0003-0793-7333

References

Adriani, O., Akaike, Y., Asano, K., et al. 2019, PhRvL, 122, 181102
Adriani, O., Barbarino, G. C., Bazilevskaya, G. A., et al. 2011, Sci, 332, 69
Adriani, O., Barbarino, G. C., Bazilevskaya, G. A., et al. 2013, ApJ, 765, 91
Agostinelli, S., Allison, J., Amako, K., et al. 2003, NIMPA, 506, 250
Aguilar, M., Aisa, D., Alpat, B., et al. 2015, PhRvL, 114, 171103
Aguilar, M., Cavasonza, L. A., Ambrosi, G., et al. 2021, PhRvL, 127, 271102
Amato, E., & Blasi, P. 2018, AdSpR, 62, 2731
Ambrosi, G., Bartocci, S., Basara, L., et al. 2020, NIMPA, 974, 164170
Ambrosi, G., Bartocci, S., Basara, L., et al. 2021, NIMPA, 1013, 165639
An, Q., Asfandiyarov, R., Azzarello, P., et al. 2019, SciA, 5, eaax3793

Aslam, O. P. M., Bisschoff, D., Ngobeni, M. D., et al. 2021, ApJ, 909, 215
Bartocci, S., Battiston, R., Burger, W. J., et al. 2020, ApJ, 901, 8
Blasi, P. 2013, A&A, 21, 70
Blasi, P. 2014, BrJPh, 44, 426
Blum, K., Katz, B., & Waxman, E. 2013, PhRvL, 111, 211101
Boezio, M., Munini, R., & Picozza, P. 2020, PrPNP, 112, 103765
Boschini, M. J., Della Torre, S., Gervasi, M., La Vacca, G., & Rancoita, P. G. 2019, AdSpR, 64, 2459
Corti, C., Potgieter, M. S., Bindi, V., et al. 2019, ApJ, 871, 253
D'Agostini, G. 1995, NIMPA, 362, 487
D'Agostini, G. 2010, arXiv:1010.0632
Donato, F., Maurin, D., Brun, P., Delahaye, T., & Salati, P. 2009, PhRvL, 102, 071301
Fisk, L. A., & Gloeckler, G. 2012, ApJ, 744, 127
Forbush, S. E. 1937, PhRv, 51, 1108
Fox, N. J., Velli, M. C., Bale, S. D., et al. 2016, SSRv, 204, 7
Gleeson, L. J., & Axford, W. I. 1968, ApJ, 154, 1011
Heber, B. 2013, SSRv, 176, 265
Hoeksema, J. T. 1992, in Solar Wind Seven Colloquium, ed. E. Marsch & R. Schwenn (Oxford: Pergamon), 191
Kóta, J. 2013, SSRv, 176, 391
Krainev, M., Kalinin, M., Aslam, O. P. M., Ngobeni, D., & Potgieter, M. S. 2021, AdSpR, 68, 2953
Marcelli, N., Boezio, M., Lenni, A., et al. 2020, ApJ, 893, 145
Marcelli, N., Boezio, M., Lenni, A., et al. 2022, ApJL, 925, L24
Martucci, M., Bartocci, S., Battiston, R., et al. 2022, PhRvD, 105, 062001
Martucci, M., Laurenza, M., Benella, S., et al. 2023, SpWea, 21, e2022SW003191
Martucci, M., Munini, R., Boezio, M., et al. 2018, ApJL, 854, L2
McComas, D. J., Alexander, N., Angold, N., et al. 2016, SSRv, 204, 187
Müller-Mellin, R., Kunow, H., Fleißner, V., et al. 1995, SoPh, 162, 483
Ngobeni, M. D., Aslam, O. P. M., Bisschoff, D., et al. 2020, Ap&SS, 365, 182
Palma, F., Sotgiu, A., Parmentier, A., et al. 2021, Appl. Sci., 11, 5680
Panov, A. D., Adams, J. H., Ahn, H. S., et al. 2009, BRASP, 73, 564
Parker, E. N. 1958, ApJ, 128, 664
Parker, E. N. 1965, P&SS, 13, 9
Picozza, P., Battiston, R., Ambrosi, G., et al. 2019, ApJS, 243, 16
Picozza, P., Galper, A., Castellini, G., et al. 2007, APh, 27, 296
Piersanti, M., Del Moro, D., Parmentier, A., et al. 2022, SpWea, 20, e2021SW003016
Potgieter, M. 2017, AdSpR, 60, 848
Potgieter, M. S. 2013, SSRv, 176, 165
Potgieter, M. S., Aslam, O. P. M., Bisschoff, D., & Ngobeni, D. 2021, MDPI Physics, 3, 1190
Potgieter, M. S., & Vos, E. E. 2017, A&A, 601, A23
Potgieter, M. S., Vos, E. E., Boezio, M., et al. 2014, SoPh, 289, 391
Quenby, J. J. 1984, SSRv, 37, 201
Ross, E., & Chaplin, W. J. 2019, SoPh, 294, 8
Shen, X., Zhang, X., Yuan, S., et al. 2018, Science China Technological Sciences, 61, 634
Shen, Z. N., Qin, G., Zuo, P., & Wei, F. 2019, ApJ, 887, 132
Song, X., Luo, X., Potgieter, M. S., Liu, X., & Geng, Z. 2021, ApJS, 257, 48
Sotgiu, A., De Donato, C., Fornaro, C., et al. 2020, Software: Practice and Experience, 51, 1459
Stephens, G. K., Morrison, D., Barnes, R. J., Potter, M., & Schaefer, R. K. 2017, AGUFM, 2017, SM13C
Stone, E. C., Cummings, A. C., Heikkila, B. C., & Lal, N. 2019, NatAs, 3, 1013
Stone, E. C., Cummings, A. C., McDonald, F. B., et al. 2013, Sci, 341, 150
Tsyganenko, N. A. 1995, JGR, 100, 5599
Usoskin, I. G. 2017, LRSP, 14, 3
Vos, E. E., & Potgieter, M. S. 2015, ApJ, 815, 119
Vos, E. E., & Potgieter, M. S. 2016, SoPh, 291, 2181
Yoon, Y. S., Anderson, T., Barrau, A., et al. 2017, ApJ, 839, 5